

Detection of ethanol, acetone, and propanal in TMC-1: New O-bearing complex organics in cold sources[★]

M. Agúndez¹, J.-C. Loison², K. M. Hickson², V. Wakelam³, R. Fuentetaja¹, C. Cabezas¹, N. Marcelino^{4,5},
B. Tercero^{4,5}, P. de Vicente⁵, and J. Cernicharo¹

¹ Instituto de Física Fundamental, CSIC, Calle Serrano 123, E-28006 Madrid, Spain
e-mail: marcelino.agundez@csic.es, jose.cernicharo@csic.es

² Institut des Sciences Moléculaires (ISM), CNRS, Univ. Bordeaux, 351 cours de la Libération, 33400, Talence, France
e-mail: jean-christophe.loison@u-bordeaux.fr

³ Laboratoire d'Astrophysique de Bordeaux, Univ. Bordeaux, CNRS, B18N, allée Geoffroy Saint-Hilaire, 33615 Pessac, France

⁴ Observatorio Astronómico Nacional, IGN, Calle Alfonso XII 3, E-28014 Madrid, Spain

⁵ Observatorio de Yebes, IGN, Cerro de la Palera s/n, E-19141 Yebes, Guadalajara, Spain

Received; accepted

ABSTRACT

We present the detection of ethanol ($\text{C}_2\text{H}_5\text{OH}$), acetone (CH_3COCH_3), and propanal ($\text{C}_2\text{H}_5\text{CHO}$) toward the cyanopolyne peak of TMC-1. These three O-bearing complex organic molecules are known to be present in warm interstellar clouds, but had never been observed in a starless core. The addition of these three new pieces to the puzzle of complex organic molecules in cold interstellar clouds stresses the rich chemical diversity of cold dense cores in stages prior to the onset of star formation. The detections of ethanol, acetone, and propanal were made in the framework of QUIJOTE, a deep line survey of TMC-1 in the Q band that is being carried out with the Yebes 40m telescope. We derive column densities of $(1.1 \pm 0.3) \times 10^{12} \text{ cm}^{-2}$ for $\text{C}_2\text{H}_5\text{OH}$, $(1.4 \pm 0.6) \times 10^{11} \text{ cm}^{-2}$ for CH_3COCH_3 , and $(1.9 \pm 0.7) \times 10^{11} \text{ cm}^{-2}$ for $\text{C}_2\text{H}_5\text{CHO}$. The formation of these three O-bearing complex organic molecules is investigated with the aid of a detailed chemical model which includes gas and ice chemistry. The calculated abundances at a time around $2 \times 10^5 \text{ yr}$ are in reasonable agreement with the values derived from the observations. The formation mechanisms of these molecules in our chemical model are as follows. Ethanol is formed on grains by addition of atomic carbon on methanol followed by hydrogenation and non-thermal desorption. Acetone and propanal are produced by the gas-phase reaction between atomic oxygen and two different isomers of the C_3H_7 radical, where the latter follows from the hydrogenation of C_3 on grains followed by non-thermal desorption. A gas-phase route involving the formation of $(\text{CH}_3)_2\text{COH}^+$ through several ion-neutral reactions followed by its dissociative recombination with electrons do also contribute to the formation of acetone.

Key words. astrochemistry – line: identification – ISM: individual objects (TMC-1) – ISM: molecules – radio lines: ISM

1. Introduction

Interstellar clouds are known to host a wide variety of complex organic molecules (COMs). Among them there are several O-bearing species with a high degree of hydrogenation, such as dimethyl ether, methyl formate, ethanol, acetone, and acetic acid, that are well known on Earth because they are used in organic chemistry laboratories. These species have been traditionally observed in warm interstellar regions, such as hot cores, hot corinos, and Galactic center clouds (Blake et al. 1987; Cazaux et al. 2003; Requena-Torres et al. 2006), where they are thought to be formed on dust grains and released to the gas phase upon thermal desorption (Garrod et al. 2008).

In recent years, O-bearing complex organic molecules typical of warm clouds, such as methyl formate (HCOOCH_3) and dimethyl ether (CH_3OCH_3), have been also observed in cold clouds (Öberg et al. 2010; Cernicharo et al. 2012; Bacmann et al. 2012; Taquet et al. 2017; Jiménez-Serra et al. 2016; Soma et

al. 2018; Agúndez et al. 2019, 2021). These detections came as a surprise because the mechanism responsible for the formation of these molecules in warm sources, which relies on the mobility of heavy radicals on grain surfaces and the thermal desorption of ices, is closed at the very low temperatures of these sources, typically around 10 K. Several scenarios have been proposed (e.g., Vasyunin & Herbst 2013; Ruaud et al. 2015; Balucani et al. 2015; Shingledecker et al. 2018; Jin & Garrod 2020), although there is not yet consensus on which if any is the correct one. Thus, the formation of methyl formate and dimethyl ether in cold sources continues to be an open problem in astrochemistry (Herbst & Garrod 2022).

In addition to methyl formate and dimethyl ether, two new O-bearing COMs, propanal ($\text{C}_2\text{H}_5\text{CHO}$) and vinyl alcohol ($\text{C}_2\text{H}_3\text{OH}$), were reported recently in the cold starless core TMC-1 (Agúndez et al. 2021). Here we report the detection of three new O-bearing COMs toward TMC-1: ethanol ($\text{C}_2\text{H}_5\text{OH}$), acetone (CH_3COCH_3), and propanal ($\text{C}_2\text{H}_5\text{CHO}$). These three molecules are well known in warm interstellar clouds (Snyder et al. 2002; Hollis et al. 2004; Requena-Torres et al. 2006; Lykke et al. 2017; Manigand et al. 2020) but have never been observed in a cold source. We also present a detailed chemical model to investigate the formation of these O-bearing COMs in TMC-1.

[★] Based on observations carried out with the Yebes 40m telescope (projects 19A003, 20A014, 20D023, 21A011, and 21D005). The 40m radio telescope at Yebes Observatory is operated by the Spanish Geographic Institute (IGN; Ministerio de Transportes, Movilidad y Agenda Urbana).

Table 1. Observed line parameters in TMC-1.

Molecule	Transition	ν_{calc} (MHz)	E_{up} (K)	$T_{b,\text{calc}}^a$ (mK)	V_{LSR}^b (km s ⁻¹)	$\Delta\nu^b$ (km s ⁻¹)	$T_A^* \text{ peak}^b$ (mK)	$\int T_A^* dv^b$ (mK km s ⁻¹)	S/N ^c (σ)
C ₂ H ₅ OH	4 _{1,3} -4 _{0,4}	32742.830	9.9	3.68	5.57 ± 0.12	1.03 ± 0.24	0.67 ± 0.17	0.73 ± 0.16	7.2
	5 _{1,4} -5 _{0,5}	36417.242	14.3	2.31	5.83 ± 0.09	1.49 ± 0.22	0.76 ± 0.12	1.21 ± 0.15	14.7
	1 _{1,1} -0 _{0,0}	43026.811	2.1	4.62	5.76 ± 0.04	1.09 ± 0.07	1.90 ± 0.18	2.21 ± 0.15	22.8
	4 _{0,4} -3 _{1,3}	46832.826	8.4	3.14	5.68 ± 0.03	0.90 ± 0.06	2.38 ± 0.23	2.28 ± 0.15	21.1
CH ₃ COCH ₃	3 _{0,3} -2 _{1,2} <i>EE</i>	33562.123	3.6	1.11	5.87 ± 0.14	0.99 ± 0.25	0.40 ± 0.13	0.42 ± 0.11	5.6
	3 _{0,3} -2 _{1,2} <i>AA</i>	33566.289	3.6	0.75	5.46 ± 0.10	0.90 ± 0.16	0.46 ± 0.12	0.44 ± 0.09	6.6
	3 _{1,3} -2 _{0,2} <i>EE</i>	34092.973	3.6	1.15	5.89 ± 0.17	1.36 ± 0.40	0.44 ± 0.15	0.64 ± 0.16	6.3
	2 _{2,1} -1 _{1,0} <i>EE</i>	35381.289	2.7	0.85	–	–	–	–	– ^d
	4 _{0,4} -3 _{1,3} <i>EE</i>	43597.127	5.7	1.54	5.95 ± 0.07	0.90 ± 0.16	0.79 ± 0.17	0.76 ± 0.12	9.2
	4 _{0,4} -3 _{1,3} <i>AA</i>	43604.463	5.7	0.61	–	–	–	–	– ^e
	4 _{1,4} -3 _{0,3} <i>AE</i>	43680.468	5.8	0.61	–	–	–	–	– ^f
	4 _{1,4} -3 _{0,3} <i>EE</i>	43689.327	5.7	1.54	5.73 ± 0.08	0.50 ± 0.17	0.61 ± 0.17	0.33 ± 0.10	5.4
	4 _{1,4} -3 _{0,3} <i>AA</i>	43698.504	5.7	1.03	5.84 ± 0.11	0.74 ± 0.24	0.71 ± 0.21	0.55 ± 0.16	6.0
	3 _{2,2} -2 _{1,1} <i>EE</i>	45233.560	4.6	0.94	–	–	–	–	– ^e
C ₂ H ₅ CHO	4 _{0,4} -3 _{1,3}	32897.820	5.0	0.72	–	–	–	–	– ^d
	3 _{1,2} -2 _{1,1}	33346.830	3.8	0.96	5.59 ± 0.15	0.99 ± 0.26	0.38 ± 0.10	0.40 ± 0.11	6.9
	3 _{1,3} -2 _{0,2}	39061.035	3.4	1.10	5.78 ± 0.10	0.79 ± 0.20	0.45 ± 0.15	0.38 ± 0.09	5.3
	4 _{1,4} -3 _{1,3}	39177.138	5.3	1.26	5.93 ± 0.10	0.73 ± 0.18	0.46 ± 0.15	0.36 ± 0.09	5.2
	4 _{0,4} -3 _{0,3}	40915.768	5.0	1.47	5.81 ± 0.12	1.11 ± 0.31	0.59 ± 0.16	0.70 ± 0.16	7.9
	4 _{2,3} -3 _{2,2}	41883.719	7.2	0.78	–	–	–	–	– ^f
	4 _{2,2} -3 _{2,1}	42936.277	7.3	0.80	–	–	–	–	– ^e
	5 _{0,5} -4 _{1,4}	44189.959	7.4	0.97	–	–	–	–	– ^f
	4 _{1,3} -3 _{1,2}	44319.499	5.9	1.30	6.07 ± 0.07	0.56 ± 0.19	0.67 ± 0.18	0.40 ± 0.11	5.8
	4 _{1,4} -3 _{0,3}	47195.073	5.3	1.31	5.90 ± 0.11	0.89 ± 0.29	0.92 ± 0.25	0.88 ± 0.22	7.6
	5 _{1,5} -4 _{1,4}	48801.725	7.6	1.40	5.63 ± 0.11	0.60 ± 0.19	0.79 ± 0.28	0.51 ± 0.16	4.9

^a $T_{b,\text{calc}}$ is the peak brightness temperature calculated in local thermodynamic equilibrium (LTE) for a rotational temperature of 6.0 K. We adopted the column density and line width derived for each molecule (see Sec. 3).

^b The line parameters V_{LSR} , $\Delta\nu$, $T_A^* \text{ peak}$, and $\int T_A^* dv$ and the associated errors are derived from a Gaussian fit to each line profile. $\Delta\nu$ is the full width at half maximum (FWHM).

^c The signal-to-noise ratio is computed as $S/N = \int T_A^* dv / [\text{rms} \times \sqrt{\Delta\nu \times \delta\nu(c/\nu_{\text{calc}})}]$, where c is the speed of light, $\delta\nu$ is the spectral resolution (0.03815 MHz), the rms is given in the uncertainty of $T_A^* \text{ peak}$, and the rest of parameters are given in the table.

^d Line is only marginally detected.

^e Line is not detected. Expected intensity is within the noise level.

^f Line is not detected. It overlaps with a frequency-switching negative artifact.

2. Astronomical observations

The data presented here are part of QUIJOTE (Q-band Ultrasensitive Inspection Journey to the Obscure TMC-1 Environment; Cernicharo et al. 2021), which is an ongoing Q-band line survey carried out with the Yebes 40m telescope at the position of the cyanopolyne peak of TMC-1 ($\alpha_{J2000} = 4^{\text{h}}41^{\text{m}}41.9^{\text{s}}$ and $\delta_{J2000} = +25^{\circ}41'27.0''$). Details on the line survey are given in previous papers of the QUIJOTE series (e.g., Cernicharo et al. 2021), while the data reduction procedure adopted is explained in Cernicharo et al. (2022). Briefly, QUIJOTE uses a 7 mm receiver covering the Q band (31.0-50.3 GHz) connected to a fast Fourier transform spectrometer providing a spectral resolution of 38.15 kHz (see Tercero et al. 2021). The data presented here correspond to observations carried out from November 2019 to November 2022, which amount to a total on-source telescope time of 758 h. The frequency-switching technique was used with frequency throws of 8 and 10 MHz. The intensity scale adopted is antenna temperature, T_A^* . The estimated uncertainty due to calibration in T_A^* is 10 %. The antenna temperature can be converted to main beam brightness temperature, T_{mb} , by dividing by $B_{\text{eff}}/F_{\text{eff}}$, where B_{eff} and F_{eff} are the beam and forward efficiencies, respectively. For the Yebes 40m telescope in the Q band, B_{eff} can be fitted as a function of frequency as $B_{\text{eff}} = 0.797 \exp[-(\nu(\text{GHz})/71.1)^2]$ using the values measured in 2022 that are reported in the webpage of the Yebes 40m tele-

scope¹, while measured values of F_{eff} range from 0.9 to 0.97 and here we adopt $F_{\text{eff}} = 0.97$. The half power beam width (HPBW) is given by $\text{HPBW}('') = 1763/\nu(\text{GHz})$. All data were analyzed using GILDAS².

3. Results

3.1. Ethanol (C₂H₅OH)

Ethanol has two conformers, *anti* and *gauche*, depending on the orientation of the OH group. The most stable and the one reported here is the *anti* form, the spectroscopy of which was taken from the Cologne Database for Molecular Spectroscopy (Müller et al. 2005)³, which in turn is based on Pearson et al. (2008) and Müller et al. (2016). The dipole moment along the b axis (all transitions observed here are b -type) is 1.438 D (Takano et al. 1968).

We detected the four lines of *anti* ethanol that are predicted to be the most intense in the Q band (see Table 1 and Fig. 1). The three lines lying at 36417 MHz, 43026 MHz, and 46832 MHz are detected with very high signal-to-noise ratios (S/N), ≥ 15 , and are precisely centered around the systemic velocity of the source, $V_{\text{LSR}} = 5.83 \text{ km s}^{-1}$ (Cernicharo et al. 2020). The

¹ https://rt40m.oan.es/rt40m_en.php

² <http://www.iram.fr/IRAMFR/GILDAS/>

³ <https://cdms.astro.uni-koeln.de/>

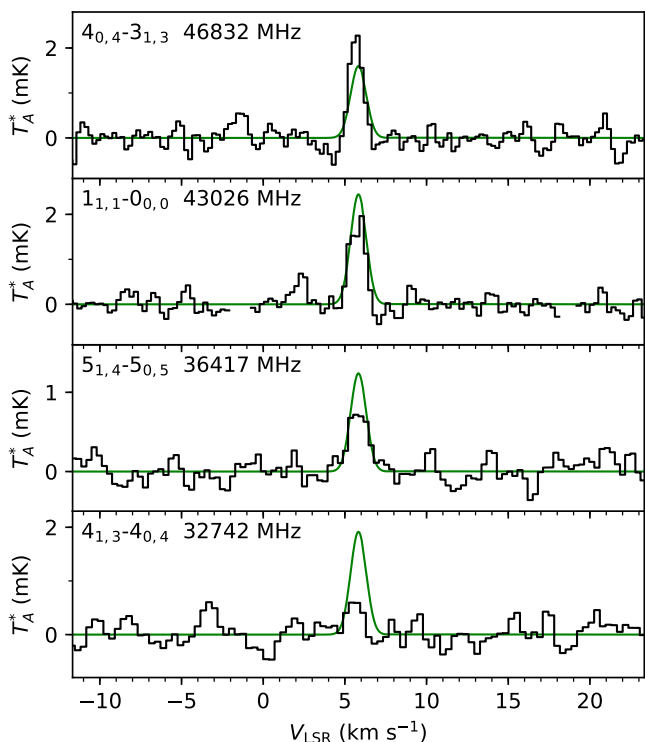


Fig. 1. Lines of C_2H_5OH observed in TMC-1 (see parameters in Table 1). In green we show the calculated spectra for $N = 1.1 \times 10^{12} \text{ cm}^{-2}$, $T_{\text{rot}} = 6.0 \text{ K}$, $\text{FWHM} = 1.13 \text{ km s}^{-1}$, and $\theta_s = 80''$.

line at 32742 MHz is also well detected although at a lower S/N and with an intensity lower than predicted by LTE. For a rotational temperature of 6.0 K, as derived below for C_2H_5OH , the predicted relative intensities for the four lines, in order of increasing frequency, are 0.80 : 0.50 : 1.00 : 0.68. From the observed velocity-integrated intensities (see Table 1), the resulting relative intensities are 0.33 : 0.55 : 1.00 : 1.03. The most puzzling point is that the first line should be at least twice more intense than it is observed. We do not have a fully satisfactory explanation for this point. It could happen that some weak line lying at $\pm 8 \text{ MHz}$ and/or $\pm 10 \text{ MHz}$ could produce a frequency switching negative artifact at the position of the 32742 MHz line, decreasing its intensity. Alternatively, non-LTE excitation effects may be playing a role. In spite of this puzzling issue on the relative intensity of the 32742 MHz line, we consider that the detection of ethanol in TMC-1 should be secure because it would be very unlikely to have four unidentified lines that by coincidence lie at the precise frequencies of the four strongest transitions of C_2H_5OH . We note that the only previous detection of ethanol in a cold source, reported toward L483 by Agúndez et al. (2019), relied on one single line.

From a rotation diagram using the four lines of ethanol detected in TMC-1 we derive a rotational temperature (T_{rot}) of $6.0 \pm 0.8 \text{ K}$ and a column density of $(1.1 \pm 0.3) \times 10^{12} \text{ cm}^{-2}$, where we assumed a circular emission distribution with a diameter $\theta_s = 80''$ (Fossé et al. 2001). The calculated line profiles are shown in Fig. 1, where we adopted as line width the arithmetic mean of the observed Δv values.

3.2. Acetone (CH_3COCH_3)

Acetone is an asymmetric rotor in which the large amplitude internal motion of the two equivalent methyl groups leads to

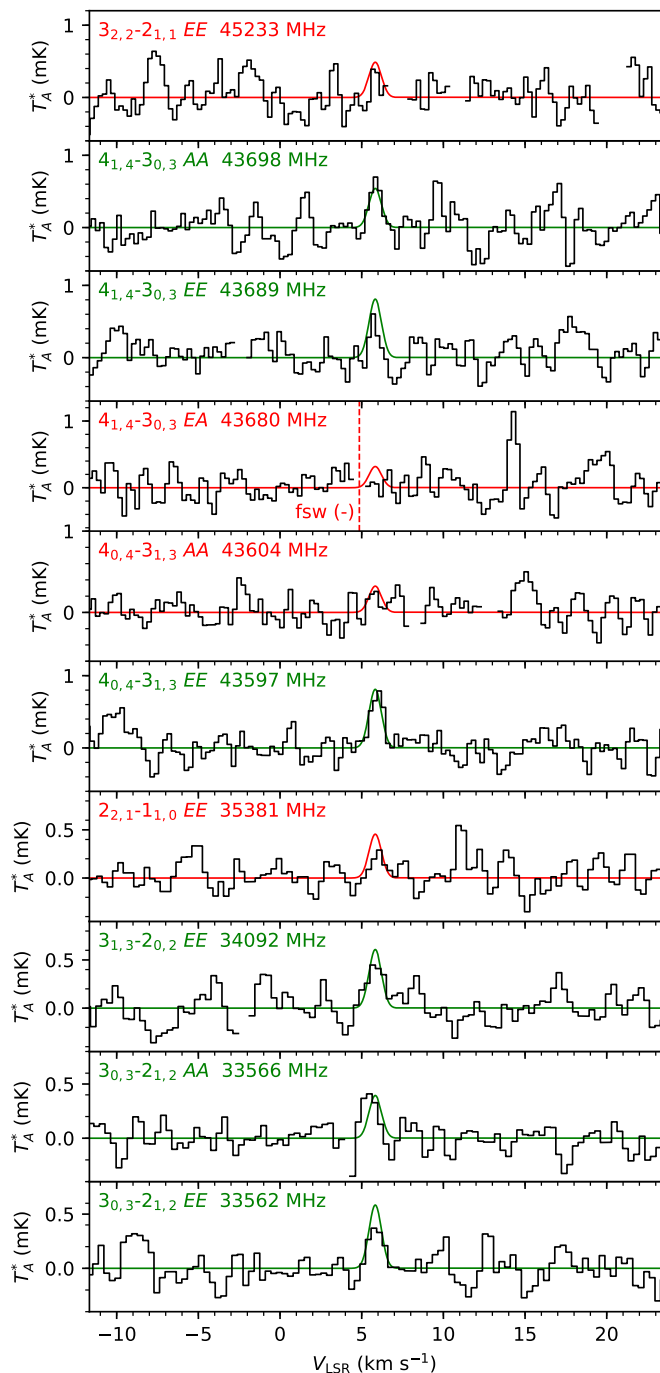


Fig. 2. Lines of CH_3COCH_3 observed in TMC-1 are shown from bottom to top in order of increasing frequency (see Table 1). The panels in green show the lines that are well detected, while those in red show lines that are not clearly detected due to a variety of reasons (see text and caption in Table 1). The position of a negative frequency switching artifact is indicated by a dashed vertical line and labeled as fsw (-). The green/red solid lines correspond to the calculated spectra for $N = 1.4 \times 10^{11} \text{ cm}^{-2}$, $T_{\text{rot}} = 6.0 \text{ K}$, $\text{FWHM} = 0.90 \text{ km s}^{-1}$, and $\theta_s = 80''$.

level splitting into AA, EE, EA, and AE substates (Groner et al. 2002), as occurs for dimethyl ether. We adopted the spectroscopy from the Jet Propulsion Laboratory (JPL) catalogue (Pickett et al. 1998)⁴. The geometry of the molecule results in a nonzero

⁴ <https://spec.jpl.nasa.gov/>

dipole moment only along the b axis, with a measured value of 2.93 D (Peter & Dreizler 1965).

We computed the line intensities of CH_3COCH_3 in LTE adopting a rotational temperature of 6.0 K, as derived for $\text{C}_2\text{H}_5\text{OH}$, and focused on the ten lines predicted to be the most intense in the Q band (see Table 1 and Fig. 2). The five most intense predicted lines within this group (those with $T_{b,\text{calc}} > 1.0$ mK; see Table 1) are all detected with low to moderate S/N, in the range $5\text{-}9\sigma$. Among the next five lines, predicted with $T_{b,\text{calc}}$ in the range $0.6\text{-}1.0$ mK (see Table 1), we only detected clearly one line, the one lying at 33566 MHz. There is another line at 35381 MHz predicted with a similar intensity which is detected only marginally (see Fig. 2). The three remaining lines lie above 40 GHz, where the sensitivity of the QUIJOTE data is worse than at lower frequencies. None of these three lines are clearly detected, although the observed spectra is consistent with the expected line intensities. For example, the lines at 43604 MHz and 45233 MHz are predicted with an intensity within the noise level of the data (see Fig. 2), while the line at 43680 MHz is not seen because there is a frequency-switching negative artifact which lies very close to the expected position of this line (see Fig. 2). In summary, among the set of ten lines predicted to be the most intense, we detected six lines with low to moderate S/N, while the four remaining lines are not detected because insufficient sensitivity or overlap with a negative frequency-switching artifact. From our experience in the detection of molecules through weak lines with the QUIJOTE data (e.g., Agúndez et al. 2021), we consider that the detection of CH_3COCH_3 is secure because it would be very unlikely to have six lines of other species precisely centered at the frequencies of the strongest lines of acetone.

The six detected lines cover a low range of upper level energies and their velocity-integrated intensities have non negligible errors, which makes it difficult to precisely determine the rotational temperature of CH_3COCH_3 . We therefore adopted a rotational temperature of 6.0 K, as determined for $\text{C}_2\text{H}_5\text{OH}$, and a source size with a diameter of $80''$, as adopted for $\text{C}_2\text{H}_5\text{OH}$, and derived a column density of $(1.4 \pm 0.6) \times 10^{11} \text{ cm}^{-2}$ for CH_3COCH_3 . The calculated line profiles, adopting as line width the average of the Δv values observed, are shown in Fig. 2.

3.3. Propanal ($\text{C}_2\text{H}_5\text{CHO}$)

Propanal has two conformers, *syn* and *gauche*, depending on the orientation of the CHO group. The most stable one is the *syn* form, which is the one detected in TMC-1. The rotational spectroscopy was taken from the CDMS (Müller et al. 2005), which is mostly based on Zingsheim et al. (2017). The components of the dipole moment along the a and b axes are 1.71 D and 1.85 D, respectively (Butcher & Wilson 1964). Both a - and b -type transitions are observed here.

Similarly to the case of acetone, we computed the line intensities in LTE of *syn* propanal assuming a rotational temperature of 6.0 K and focused on the lines expected with a brightness temperature $T_{b,\text{calc}}$ above 0.7 mK. The eleven resulting lines are given in Table 1 and shown in Fig. 3. There are eight lines within this selected group which are predicted with $T_{b,\text{calc}} > 0.9$ mK, from which we detected seven lines with low to moderate S/N in the range $5\text{-}8\sigma$. The remaining line at 44189 MHz overlaps with a negative artifact resulting from the frequency-switching technique (see Fig. 3). The other four lines predicted to be less intense, with $T_{b,\text{calc}}$ in the range $0.7\text{-}0.9$ mK are not clearly detected for different reasons. The line at 32897 MHz is only marginally detected, while the one at 41883 MHz overlaps with a frequency-switching negative artifact, and the last

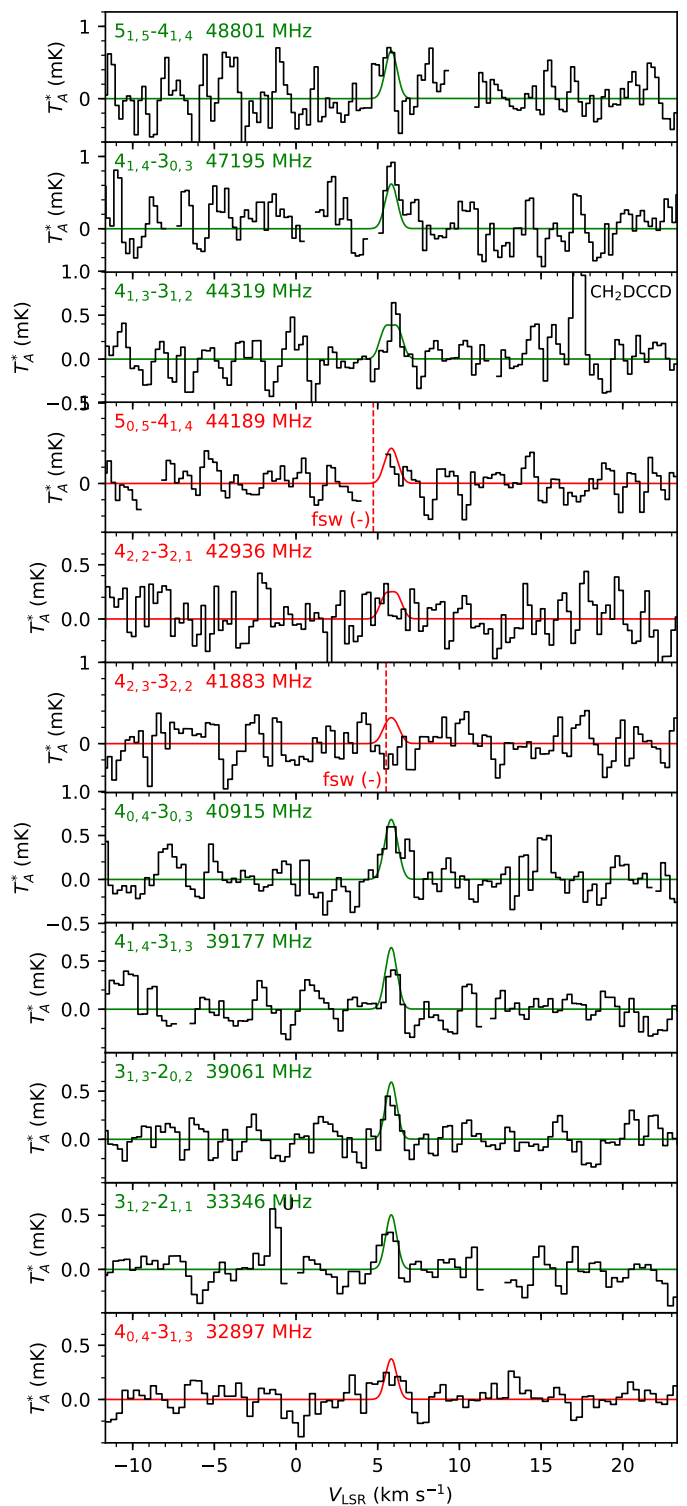


Fig. 3. Same as Fig. 2 but for $\text{C}_2\text{H}_5\text{CHO}$, i.e. detected lines in green and non detected lines in red (see line parameters in Table 1). The green/red solid lines correspond to the calculated spectra for $N = 1.9 \times 10^{11} \text{ cm}^{-2}$, $T_{\text{rot}} = 6.0$ K, FWHM = 0.81 km s^{-1} , and $\theta_s = 80''$.

one at 42936 MHz is predicted with an intensity within the noise level of the data. Even if the lines of propanal are detected with relatively low S/N, we are confident about the detection due to the high number of detected lines (seven) and because we can explain those lines which are not detected on the basis of insufficient sensitivity or overlap with negative artifacts from the

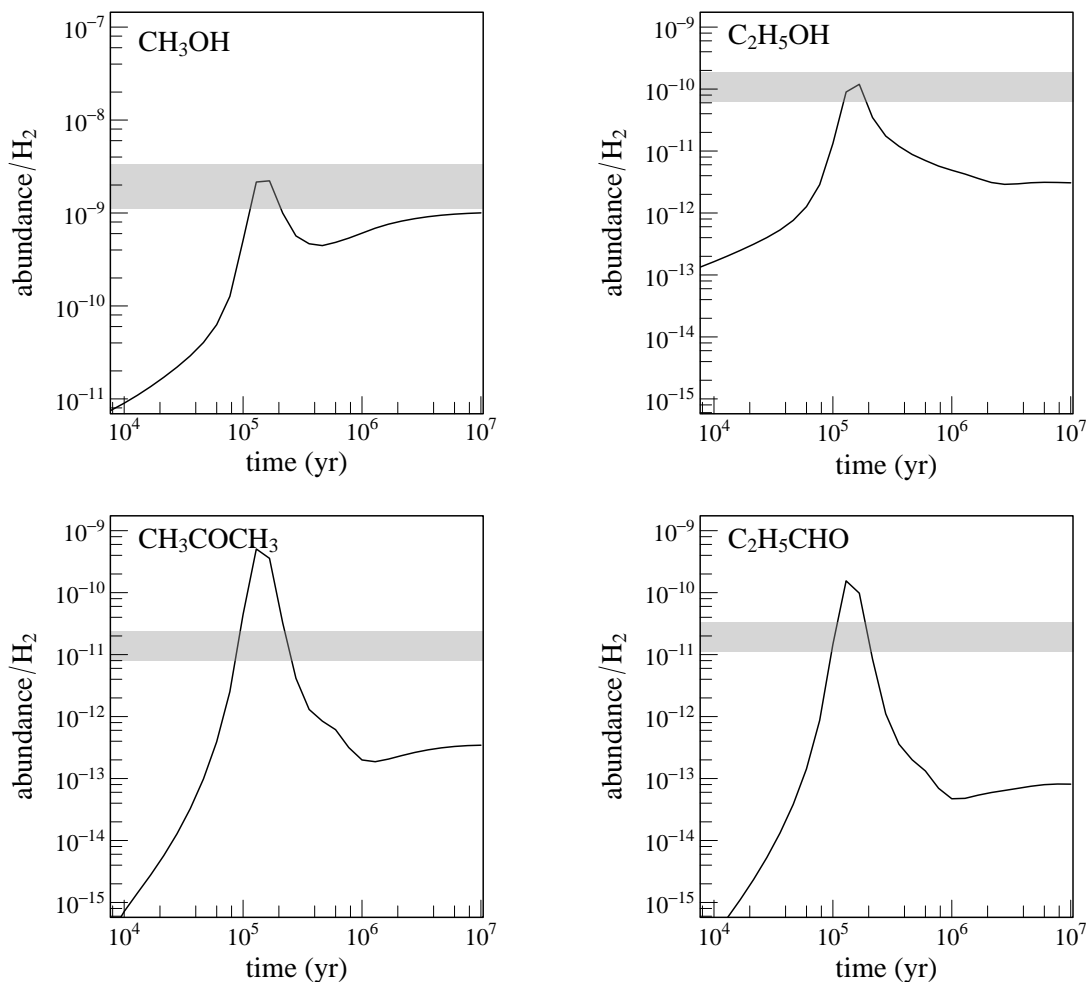


Fig. 4. Abundances of CH_3OH , $\text{C}_2\text{H}_5\text{OH}$, CH_3COCH_3 , and $\text{C}_2\text{H}_5\text{CHO}$ as a function of time calculated with our chemical model. The horizontal grey rectangles represent the abundances observed in TMC-1 assuming an uncertainty of a factor of three.

frequency-switching observing mode. As in the case of acetone, it will be very unlikely to have seven lines from different species located at the precise frequencies of the most intense lines of *syn* propanal.

As in the case of acetone, the sizable errors in the velocity-integrated intensities do not allow to constrain precisely the rotational temperature of propanal. We therefore adopted a rotational temperature of 6.0 K, as determined for $\text{C}_2\text{H}_5\text{OH}$. As with the previous molecules, we adopt an emission distribution with a diameter of $80''$. The column density derived for $\text{C}_2\text{H}_5\text{CHO}$ is $(1.9 \pm 0.7) \times 10^{11} \text{ cm}^{-2}$. In Fig. 3 we show the line profiles computed, where we adopted as FWHM the mean of the Δv values observed.

4. Chemical model

To describe the chemistry of O-bearing COMs in TMC-1 we used the Nautilus code, which is a three-phase (gas, dust grain ice surface, and dust grain ice mantle) time-dependent chemical model (Ruaud et al. 2016). The code has been recently updated with a better description of the chemistry of COMs in the gas phase and on grains (Manigand et al. 2021; Coutens et al. 2022) and with the inclusion of sputtering of ices by cosmic-rays (Wakelam et al. 2021). To describe the physical conditions in TMC-1 we use an homogeneous cloud with an H_2 volume

density of $2.5 \times 10^4 \text{ cm}^{-3}$, a temperature of 10 K for both gas and dust, a visual extinction of 30 mag, and a cosmic-ray ionization rate of H_2 of $1.3 \times 10^{-17} \text{ s}^{-1}$. All elements are assumed to be initially in atomic form, except for hydrogen, which is entirely molecular. The initial abundances are those of Table 1 of Hincelin et al. (2011), the C/O elemental ratio being equal to 0.7 in that study.

The calculated abundances relative to H_2 for the O-bearing COMs detected in this study are shown in Fig. 4. The observed abundances are relatively well reproduced by the model for a cloud age around $2 \times 10^5 \text{ yr}$. It should be noted that although the destruction pathways of COMs are fairly well constrained, this is not the case for the formation pathways. Destruction of COMs occurs mainly through reactions with H_3^+ and atomic carbon. The reactions with H_3^+ are an important destruction pathway for COMs because not only is the protonated form usually a minor product (Lee et al. 1992), but also the electronic dissociative recombination (DR) of the protonated form gives back very little of the original COM. For example, the DR of $\text{C}_2\text{H}_5\text{OH}_2^+$ produces less than 7% of $\text{C}_2\text{H}_5\text{OH}$ (Hamberg et al. 2010). The reactions with C are also an important destruction pathway for COMs because atomic carbon seems to react without a barrier with numerous COMs (Husain & Ioannou 1999; Shannon et al. 2014; Hickson et al. 2021). The other important destruction pathways are the reactions with C^+ , H^+ , S^+ , and He^+ . With regard

to the formation of O-bearing COMs in cold molecular clouds, there are several very different possible pathways.

First, bimolecular reactions between atomic oxygen and hydrocarbon radicals can be an important source of O-bearing COMs. Since atomic oxygen is very abundant, this mechanism can be very efficient when the hydrocarbon radical is present with a high enough abundance. Acetone is produced through the $O + 2\text{-C}_3\text{H}_7$ (CH_3CHCH_3) reaction and propanal is produced through the $O + 1\text{-C}_3\text{H}_7$ ($\text{CH}_2\text{CH}_2\text{CH}_3$) reaction (Tsang & Hampson 1986; Hoyermann & Sievert 1979). In our present version of the model we consider that C_3 does not react with oxygen atoms (Woon & Herbst 1996), which results in high abundances of C_3 derivatives in the ice (Hickson et al. 2016) and a notable abundance for the C_3H_7 radical in the gas phase through chemical desorption (Garrod et al. 2007; Minissale et al. 2016) and cosmic-ray sputtering (Wakelam et al. 2021). This is the main formation pathway for $\text{C}_2\text{H}_5\text{CHO}$ and an important one for CH_3COCH_3 .

Second, radiative association between neutral radicals can directly produce O-bearing COMs. For example, the association of CH_3 and CH_2OH can yield $\text{C}_2\text{H}_5\text{OH}$, while $\text{CH}_3 + \text{CH}_3\text{CO}$ can form CH_3COCH_3 . These two reactions have not been studied to the best of our knowledge but are likely to be fast by comparison with $\text{CH}_3 + \text{CH}_3\text{O} \rightarrow \text{CH}_3\text{OCH}_3 + h\nu$ (Tennis et al. 2021). However, these reactions are not very efficient in our TMC-1 model because the calculated abundances of CH_2OH and CH_3CO are too small. It would be interesting to search for CH_2OH , a species whose microwave spectroscopy has been recently studied (Bermúdez et al. 2017; Chitarra et al. 2020; Coudert et al. 2022) to see if its abundance is significantly higher than calculated, which could increase the role of radiative associations between neutrals in the synthesis of COMs, as suggested by Balucani et al. (2015).

The third way to produce O-bearing COMs is the DR of their protonated form. However, there are relatively few reactions producing the protonated form of the COMs, mostly ion-neutral radiative associations which compete with the faster proton transfer channel when this is exothermic. We used the reactions and rate coefficients from Herbst (1987) and Herbst et al. (1990) to produce $\text{C}_2\text{H}_5\text{CHO}$ and CH_3COCH_3 , reviewing the different pathways to $(\text{CH}_3)_2\text{COH}^+$, in addition to the one postulated by Herbst et al. (1990), $\text{CH}_3^+ + \text{CH}_3\text{CHO}$ (see Appendix A). In any case, these routes play a secondary role in the formation of the O-bearing COMs observed in this study except for CH_3COCH_3 , in which case the pathway initiated by the reaction $\text{OH} + \text{C}_3\text{H}_7^+$ is favored by the important production of C_3 and its derivatives.

The last possible way of production of COMs is through their synthesis on grains followed by desorption. As the majority of species are not mobile on grains at 10 K, except for atomic hydrogen and to a lesser extent atomic nitrogen, this requires an abundant precursor in the gas phase and an efficient low temperature desorption mechanism, such as chemical desorption (Garrod et al. 2007; Minissale et al. 2016) or cosmic-ray sputtering (Wakelam et al. 2021). This is the case for methanol, formed from the surface hydrogenation of CO produced in the gas phase. This is also potentially the case for C_3 derivatives (methylacetylene, propene, propane) if C_3 does not react with atomic oxygen (Woon & Herbst 1996; Hickson et al. 2016), but not for COMs in general. However, since atomic carbon reacts without barrier with species on grains such as H_2CO (Husain & Ioannou 1999) and CH_3OH (Shannon et al. 2014), the reactive sticking of carbon atom to the grains induces the formation of COMs through an Eley-Rideal mechanism, as discussed by Ruaud et al. (2015). In particular, in our model $\text{C}_2\text{H}_5\text{OH}$ is mainly formed by the in-

sertion of the C atom into the C–O bond of CH_3OH followed by hydrogenation.

In summary, our chemical model indicates that $\text{C}_2\text{H}_5\text{OH}$ is mostly produced on grains, $\text{C}_2\text{H}_5\text{CHO}$ is mainly formed by the reaction $O + 1\text{-C}_3\text{H}_7$, where $1\text{-C}_3\text{H}_7$ itself is produced on grains, while CH_3COCH_3 is produced by the $O + 2\text{-C}_3\text{H}_7$ reaction ($2\text{-C}_3\text{H}_7$ itself is produced on grains) and the DR of $(\text{CH}_3)_2\text{COH}^+$, where $(\text{CH}_3)_2\text{COH}^+$ is produced by the reactions $\text{OH} + \text{C}_3\text{H}_7^+$, $\text{H}_2\text{O} + \text{C}_3\text{H}_5^+$, and $\text{C}_2\text{H}_4 + \text{H}_2\text{COH}^+$. The agreement between the observations and the simulations for CH_3COCH_3 and $\text{C}_2\text{H}_5\text{CHO}$ is very dependent on the efficiency of the $O + \text{C}_3$ reaction and the efficiency of the desorption mechanisms. It is also indirectly dependent on the rate of the reactions of C_3H_3^+ and C_3H_5^+ with H_2 , which are very slow at room temperature (Lin et al. 2013) but could be open at low temperature due to tunneling. These hydrogenation reactions are essential to reproduce the observations of CH_3CCH (Markwick et al. 2002) and C_3H_6 (Marcelino et al. 2007), which cannot be explained by the desorption of these species alone from the grains. It is important to emphasize the role of the $O + \text{C}_3$ reaction which, if slow, allows the observed O-bearing COM abundances to be reproduced but induces a very high abundance of C_3 in the gas phase which seems incompatible with the ^{13}C fractionation of $c\text{-C}_3\text{H}_2$ (Loison et al. 2020) and the abundances of CH_3CCH and C_3H_6 around protostars (Manigand et al. 2021).

An interesting test of the ability of our chemical model to explain the chemistry of O-bearing COMs in TMC-1 is to verify if the model can account for the observed abundance of methanol. Even if the production mechanisms of methanol, ethanol, acetone, and propanal are different, the chemistry on grain surfaces is crucial for these species. It is essential for CH_3OH , $\text{C}_2\text{H}_5\text{OH}$, and $\text{C}_2\text{H}_5\text{CHO}$, and important for CH_3COCH_3 . For the three latter molecules grain surface chemistry plays a role because $\text{C}_2\text{H}_5\text{OH}$ is formed from the reaction of atomic carbon with adsorbed CH_3OH , while CH_3COCH_3 and $\text{C}_2\text{H}_5\text{CHO}$ are formed from the desorption of C_3H_x species followed by gas-phase chemistry. Similarly, the formation of methanol is essentially done on grains (more than 99%) by the successive hydrogenation of CO, with part of this methanol being injected into the gas phase by two mechanisms: desorption induced by cosmic-rays (Wakelam et al. 2021) and chemical desorption (Minissale et al. 2016). It is worth to note that the formation pathway to methanol in the gas phase from the dissociative recombination of protonated methanol is globally inefficient. On the one hand, the formation of CH_3OH_2^+ itself through either the radiative association between CH_3^+ and H_2O (Gerlich & Smith 2006) or the reaction between H_3^+ and HCOOCH_3 (Lawson et al. 2012) is not very efficient. On the other hand, the production of methanol is a minor channel in the dissociative recombination of CH_3OH_2^+ with electrons (Geppert et al. 2006). The calculated abundance of CH_3OH (see Fig. 4) shows a good agreement with the value derived from observations of TMC-1 (Pratap et al. 1997; Soma et al. 2015, 2018) for a cloud age around 2×10^5 yr, as for the other O-bearing COMs detected in this study.

5. Conclusions

We detected, for the first time in a starless core (TMC-1), three new O-bearing COMs: ethanol, acetone, and propanal. These detections enlarge the inventory of O-bearing COMs known to be present in cold interstellar clouds, where previously other molecules of this type, such as methyl formate, dimethyl ether, propenal, and vinyl alcohol have been found. These molecules are present at abundance levels of 10^{-11} - 10^{-10} with respect to H_2 in

TMC-1. A chemical model including gas and dust chemistry is able to explain the formation of ethanol, acetone, and propanal in TMC-1 based on a combination of grain chemistry, non-thermal desorption, and gas-phase chemical processes.

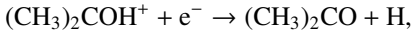
Acknowledgements. We acknowledge funding support from Spanish Ministerio de Ciencia e Innovación through grants PID2019-106110GB-I00, PID2019-107115GB-C21, and PID2019-106235GB-I00 and from the European Research Council (ERC Grant 610256: NANOCOSMOS). J.-C.L., K.H., and V.W. acknowledge the CNRS program "Physique et Chimie du Milieu Interstellaire" (PCMI) co-funded by the Centre National d'Études Spatiales (CNES). We thank the referee for a critical reading of the article.

References

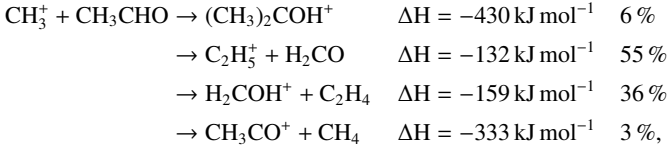
- Agúndez, M., Marcelino, N., Cernicharo, J., et al. 2019, *A&A*, 625, A147
- Agúndez, M., Marcelino, N., Tercero, B., et al. 2021, *A&A*, 649, L4
- Bacmann, A., Taquet, V., Faure, A., et al. 2012, *A&A*, 541, L12
- Balucani, N., Ceccarelli, C., & Taquet, V. 2015, *MNRAS*, 449, L16
- Bermúdez, C., Bailleux, S., & Cernicharo, J. 2017, *A&A*, 598, A9
- Blake, G. A., Sutton, E. C., Mason, C. R., & Phillips, T. G. 1987, *ApJ*, 315, 621
- Butcher, S. & Wilson, E. B. 1964, *J. Chem. Phys.*, 40, 1671
- Cazaux, S., Tielens, A. G. G. M., Ceccarelli, C., et al. 2003, *ApJ*, 593, L51
- Cernicharo, J., Marcelino, N., Roueff, E., et al. 2012, *ApJ*, 759, L43
- Cernicharo, J., Marcelino, N., Agúndez, M., et al. 2020, *A&A*, 642, L8
- Cernicharo, J., Agúndez, M., Kaiser, R. I., et al. 2021, *A&A*, 652, L9
- Cernicharo, J., Fuentetaja, R., Agúndez, M., et al. 2022, *A&A*, 663, L9
- Chitarra, O., Martin-Drumel, M.-A., Gans, B., et al. 2020, *A&A*, 644, A123
- Coudert, L. H., Chitarra, O., Spaniol, J.-T., et al. 2022, *J. Chem. Phys.*, 156, 244301
- Coutens, A., Loison, J.-C., Boulanger, A., et al. 2022, *A&A*, 660, L6
- Fossé, D., Cernicharo, J., Gerin, M., & Cox, P. 2001, *ApJ*, 552, 168
- Garrod, R. T., Wakelam, V., & Herbst, E. 2007, *A&A*, 467, 1103
- Garrod, R. T., Widicus Weaver, S. L., & Herbst, E. 2008, *ApJ*, 682, 283
- Geppert, W. D., Hamberg, M., Thomas, R. D., et al. 2006, *Faraday Discuss.*, 133, 177
- Gerlich, D. & Smith, M. 2006, *Phys. Scr.*, 73, C25
- Groner, P., Albert, S., Herbst, E., et al. 2002, *ApJS*, 142, 145
- Hamberg, M., Zhaunerchyk, V., Vigren, E., et al. 2010, *A&A*, 522, A90
- Herbst, E. 1987, *ApJ*, 313, 867
- Herbst, E., Giles, K., & Smith, D. 1990, *ApJ*, 358, 468
- Herbst, E. & Garrod, R. T. 2022, *FrASS*, 8, 209
- Hickson, K. M., Wakelam, V., & Loison, J.-C. 2016, *Mol. Astrophys.*, 3, 1
- Hickson, K. M., Loison, J.-C., & Wakelam, V. 2021, *ACS Earth Space Chem.*, 5, 824
- Hincelin, U., Wakelam, V., Hersant, F., et al. 2011, *A&A*, 530, A61
- Hollis, J. M., Jewell, P. R., Lovas, F. J., et al. 2004, *ApJ*, 610, L21
- Hoyermann, K. & Sievert, R. 1979, *Symposium (International) on Combustion*, 17, 517
- Husain, D. & Ioannou, A. X. 1999, *J. Photochem. Photobiol. A*, 129, 1
- Jiménez-Serra, I., Vasyunin, A. I., Caselli, P., et al. 2016, *ApJ*, 830, L6
- Jin, M. & Garrod, R. T. 2020, *ApJS*, 249, 26
- Lawson, P. A., Osborne, D. S., & Adams, N. G. 2012, *J. Phys. Chem. A*, 116, 2880
- Lee, H. S., Drucker, M., & Adams, N. G. 1992, *Int. J. Mass Spectrom. Ion Process.*, 117, 101
- Lin, Z., Talbi, D., Roueff, E., et al. 2013, *ApJ*, 765, 80
- Loison, J.-C., Wakelam, V., Gratier, P., & Hickson, K. M. 2020, *MNRAS*, 498, 4663
- Lykke, J. M., Coutens, A., Jørgensen, J. K., et al. 2017, *A&A*, 597, A53
- Manigand, S., Jørgensen, J. K., Calcutt, H., et al. 2020, *A&A*, 635, A48
- Manigand, S., Coutens, A., Loison, J.-C., et al. 2021, *A&A*, 645, A53
- Marcelino, N., Cernicharo, J., Agúndez, M., et al. 2007, *ApJ*, 665, L127
- Markwick, A. J., Millar, T. J., & Charnley, S. B. 2002, *A&A*, 381, 560
- Milligan, D. B., Wilson, P. F., Freeman, C. G., et al. 2002, *J. Phys. Chem. A*, 106, 9745
- Minissale, M., Dulieu, F., Cazaux, S., & Hocuk, S. 2016, *A&A*, 585, A24
- Müller, H. S. P., Schlöder, F., Stutzki, J., & Winnewisser, G. 2005, *J. Mol. Struct.*, 742, 215
- Müller, H. S. P., Belloche, A., Xu, L.-H., et al. 2016, *A&A*, 587, A92
- Öberg, K. I., Bottinelli, S., Jørgensen, J. K., & van Dishoeck, E. F. 2010, *ApJ*, 716, 825
- Pearson, J. C., Brauer, C. S., & Drouin, B. J. 2008, *J. Mol. Spectr.*, 251, 394
- Peter, R. & Dreizler, H. 1965, *Z. Naturforsch.*, 20a, 301
- Pickett, H. M., Poynter, R. L., Cohen, E. A., et al. 1998, *J. Quant. Spectr. Rad. Transf.*, 60, 883
- Pratap, P., Dickens, J. E., Snell, R. L., et al. 1997, *ApJ*, 486, 862
- Requena-Torres, M. A., Martín-Pintado, J., Rodríguez-Franco, A., et al. 2006, *A&A*, 455, 971
- Ruaud, M., Loison, J.-C., Hickson, K. M., et al. 2015, *MNRAS*, 447, 4004
- Ruaud, M., Wakelam, V., & Hersant, F. 2016, *MNRAS*, 459, 3756
- Shannon, R. J., Cossou, C., Loison, J.-C., et al. 2014, *RSC Adv.*, 4, 26342
- Shingledecker, C. N., Tennis, J., Le Gal, R., & Herbst, E. 2018, *ApJ*, 861, 20
- Snyder, L. E., Lovas, F. J., Mehringer, D. M., et al. 2002, *ApJ*, 578, 245
- Soma, T., Sakai, N., Watanabe, Y., & Yamamoto, S. 2015, *ApJ*, 802, 74
- Soma, T., Sakai, N., Watanabe, Y., & Yamamoto, S. 2018, *ApJ*, 854, 116
- Takano, M., Sasada, Y., & Satoh, T. 1968, *J. Mol. Spectr.*, 26, 157
- Tanner, S. D., Mackay, G. I., & Bohme, D. K. 1979, *Can. J. Chem.*, 57, 2350
- Taquet, V., Wirstrom, E. S., Charnley, S. B., et al. 2017, *A&A*, 607, A20
- Tennis, J., Loison, J.-C., & Herbst, E. 2021, *ApJ*, 922, 133
- Tercero, F., López-Pérez, J. A., Gallego, J. D., et al. 2021, *A&A*, 645, A37
- Tsang, W. & Hampson, R. F. 1986, *J. Phys. Chem. Ref. Data*, 15, 1087
- Vasyunin, A. I., & Herbst, E. 2013, *ApJ*, 769, 34
- Wakelam, V., Dartois, E., Chabot, M., et al. 2021, *A&A*, 652, A63
- Woon, D. E. & Herbst, E. 1996, *ApJ*, 465, 795
- Zhao, Y. & Truhlar, D. G. 2008a, *Theor. Chem. Acc.*, 120, 215
- Zhao, Y. & Truhlar, D. G. 2008b, *Acc. Chem. Res.*, 41, 157
- Zingsheim, O., Müller, H. S. P., Lewen, F., et al. 2017, *J. Mol. Spectr.*, 342, 125

Appendix A: Ionic formation pathways of CH_3COCH_3 and $\text{C}_2\text{H}_5\text{CHO}$

Herbst et al. (1990) proposed that acetone may be produced by the dissociative recombination of the ion $(\text{CH}_3)_2\text{COH}^+$,



where $(\text{CH}_3)_2\text{COH}^+$ would be formed in the reaction



for which the rate coefficient and branching ratios were measured at room temperature. The measured rate coefficient for the three-body association was used to calculate the rate coefficient of the radiative association at low temperature using phase space theory and assuming an exit barrier to the production of bimolecular products ($\text{C}_2\text{H}_5^+ + \text{H}_2\text{CO}$, $\text{H}_2\text{COH}^+ + \text{C}_2\text{H}_4$, and $\text{CH}_3\text{CO}^+ + \text{CH}_4$).

To explore other possible $(\text{CH}_3)_2\text{COH}^+$ formation pathways we performed various theoretical calculations on the global $(\text{CH}_3)_2\text{COH}^+$ potential energy surface (PES) using density functional theory (DFT) employing the M06-2X functional (Zhao &

Trular 2008a) coupled with the aug-cc-pVTZ (AVTZ) basis set. This functional has been shown to have good accuracy for the prediction of main group thermochemistry and barrier heights (Zhao & Trular 2008b). The results of our calculations are shown in Fig. A.1.

It appears that the product channels $\text{C}_2\text{H}_5^+ + \text{H}_2\text{CO}$, $\text{H}_2\text{COH}^+ + \text{C}_2\text{H}_4$, $\text{C}_3\text{H}_5^+ + \text{H}_2\text{O}$ and $\text{H}_3\text{O}^+ + \text{CH}_3\text{CCH}$ are all barrierless, which implies a decrease of the theoretical rate coefficient of the radiative association channel with respect to the value of Herbst et al. (1990), although it opens other possible pathways for the production of $(\text{CH}_3)_2\text{COH}^+$. For the $\text{C}_2\text{H}_5^+ + \text{H}_2\text{CO}$ and $\text{H}_3\text{O}^+ + \text{CH}_3\text{CCH}$ reactions, protonation was observed to proceed in the absence of competing channels (Tanner et al. 1979; Milligan et al. 2002). The $\text{CH}_3\text{CO}^+ + \text{CH}_4$ reaction involves large barriers and does not play a role in the formation of CH_3CO or $\text{C}_2\text{H}_5\text{CHO}$. The two reactions, in addition to $\text{CH}_3^+ + \text{CH}_3\text{CHO}$, that can produce the protonated forms of acetone and propanal through radiative association are $\text{H}_2\text{COH}^+ + \text{C}_2\text{H}_4$ and $\text{C}_3\text{H}_5^+ + \text{H}_2\text{O}$. The calculation of these rate coefficients is beyond the scope of this article but should be done in the future. Here we used values that seem realistic (a few $10^{-10} \text{ cm}^3 \text{ s}^{-1}$ at 10 K) and we also used the maximum rate coefficient calculated by Herbst et al. (1990), $2 \times 10^{-10} \text{ cm}^3 \text{ s}^{-1}$ at 10 K, for the reaction

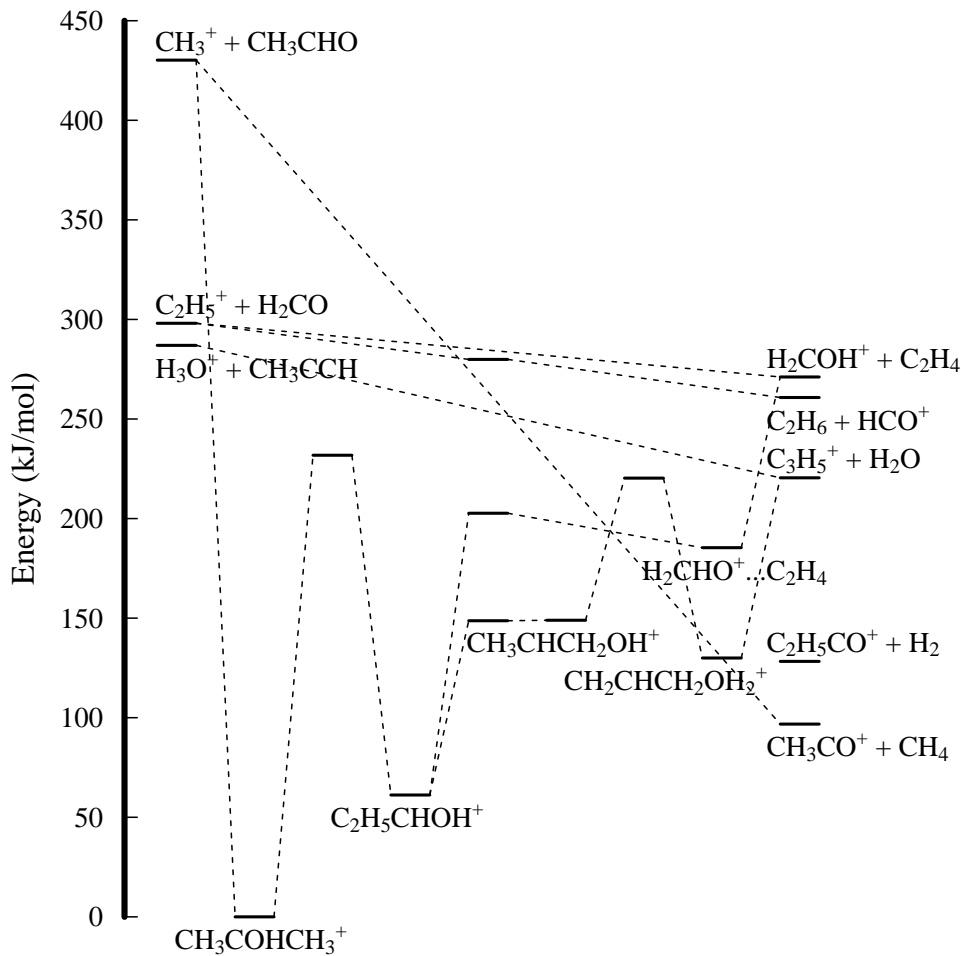
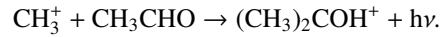
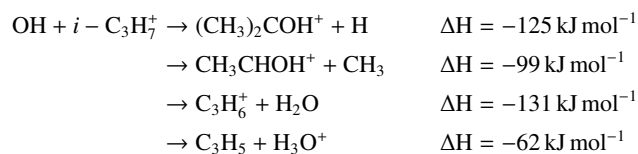


Fig. A.1. Schematic representation of the PES of $(\text{CH}_3)_2\text{COH}^+$.

However, even using these rate coefficients and considering large branching ratios (30 %) for the production of CH_3COCH_3 and $\text{C}_2\text{H}_5\text{CHO}$ by dissociative recombination of their protonated forms with electrons, the production of CH_3COCH_3 and $\text{C}_2\text{H}_5\text{CHO}$ is largely insufficient to reproduce the observations if their protonated forms are formed only by the radiative association reactions $\text{CH}_3^+ + \text{CH}_3\text{CHO}$, $\text{H}_2\text{COH}^+ + \text{C}_2\text{H}_4$, and $\text{C}_3\text{H}_5^+ + \text{H}_2\text{O}$.

An alternative route for the production of $(\text{CH}_3)_2\text{COH}^+$ is the $\text{OH} + i\text{-C}_3\text{H}_7^+$ reaction:



We studied this reaction at the M06-2X/AVTZ level and found by relaxing the geometry at each distance that the reaction producing the $\text{CH}_3\text{CHOHCH}_3^+$ adduct is barrierless. The evolution of this adduct can lead to different products including $(\text{CH}_3)_2\text{COH}^+ + \text{H}$, which is the most exothermic path with a very small barrier (or none at all) in the exit channel and therefore most likely an important if not the main product channel.